Ballooning Modes Instabilities in Outward LHD Configurations

Jacobo VARELA, Kiyomasa Y. WATANABE[1)], Noriyoshi NAKAJIMA[1)], Satoshi OHDACHI[1)], Luis GARCIA and Jose A. MIER

Universidad Carlos III, 28911 Leganés, Madrid, Spain

[1)]*National Institute for Fusion Science, Oroshi-cho 322-6, Toki 509-5292, Japan*

(Received 21 October 2010 / Accepted 2 February 2011)

The aim of this 3D ballooning mode growth rates study is to point out the existence of ballooning activity in outward LHD configurations near the edge, and to find out how these instabilities are triggered in equilibria that simulate plasmas of high density core operations with internal transport barrier. 3D ballooning mode growth rates and Mercier stability were studied for several magnetic configurations with different beta values, and the research reveals an intense activity in outward configurations near the plasma edge, where Mercier criterion predicts stability for interchange modes and experimental data situates the density collapse events [S. Ohdachi *et al.*, Contrib. Plasma Phys. **50**, 552 (2010)].

Keywords: nuclear fusion, LHD, MHD, ballooning

DOI: 10.1585/pfr.6.1403013

1. Introduction

Magnetohydrodynamic (MHD) stability behaviour is quite sensitive to the magnetic axis location in the Large Helical Device (LHD) [1]. Relative shift between the magnetic axis and the last close flux surface affects the MHD properties of the system, like the location of magnetic hill regions where the interchange modes can be triggered.

Different magnetic axis configurations have been tested in the experimental activity of LHD. Not only the interchange modes are destabilized, ballooning modes can be triggered too in configurations with a strong local bad magnetic curvature. For inward configurations, previous studies relate this activity with 3D ballooning-like instabilities [2, 3], and the mode structure was found under global MHD instability analysis using the cas3d code [4–6]. This paper had expanded the 3D ballooning study to outward configurations, where its activity looks like more restrictive to the device operation, because they are a candidate to be the main driver of density collapse events observed in outward configurations for operations with high density cores and internal transport barrier [7].

In the present paper, we have used VMEC [8] fixed boundary reconstructed equilibria, with broad $P(\psi_N) = P_0(1-\psi_N^2)^2$ and peaked $P(\psi_N) = P_0(1-\psi_N^2)$ pressure profiles, and field lines with different curvature properties. VMEC equilibria for broad pressure profile shows a better agreement than peaked profile between simulation and experimental profiles. The Mercier criterion [9] and high n global mode growth rates γ will be studied on each configuration to provide information about the instabilities nature by using the Hn-bal code [2, 10]. Hn-bal code uses the field line coordinate system (ψ, η, α), related with Boozer coordinates (ψ, θ, ξ) like $\eta = \theta$ and $\alpha = \xi - (1/\iota)\theta$, where α is the label for the magnetic field line. θ_k is the radial wave number. Hn-bal uses a sixth-order Runge-Kutta numerical method in the resolution of the ballooning equation (Appendix) [11–13].

The toroidal current is assumed zero in this research, and only the instabilities driven by pressure gradients will be considered. Destabilization due to currents is ignored as a first approximation to the problem, because in the LHD operations regimes under study the net current is nearly null and the MHD stability of the system is dominated by pressure driven modes [14]. Low n global modes are marginally unstable at the edge of the plasma for high beta operation with $\langle\beta_{dia}\rangle = 4\%$ for inward configurations [15], but in outward configuration they are stable and only high modes activity is expected. Bootstrap current is not considerated because its effects in outward configurations are negligible [16]. Fast ions effects are neglected too at first step because total flux of fast ions is smaller in outward configurations than inward configurations [17], and ballooning modes are not stabilized like for inward configurations [18].

Heliotron devices like LHD have a large Shafranov shift [19, 20] and magnetic surfaces suffer an intense deformation. Local properties such as shear and curvature are affected and the driving of instabilities depends on these equilibrium characteristics.

We want to study the stability properties of the system at the edge, and to understand the nature of the instabilities onset in this region. The goal of this study is to relate the so-called 3D ballooning modes with the MHD activity in LHD outward shifted configuration, one candidate to explain the triggering of density collapse events as their main

author's e-mail: jvrodrig@fis.uc3m.es

driver. We will carry out these comparisons by analyzing the high n ballooning modes ($n \to \infty$) for LHD configurations with several vacuum magnetic axis position and beta values in regions with good and bad magnetic curvature. In this study we have used VMEC fixed boundary equilibria for broad pressure and peaked pressure profiles [21]. For broad pressure profiles, the study has been made for two regions with different magnetic curvature.

The rest of the paper is organized as follows: In Sec. 2, we present the results of the Mercier criterion instability region versus high n global modes growth rate for several magnetic axis configurations and beta. Section 3 contains the conclusions and discussion of the paper.

2. Calculation Results

We carried out the study for configurations with magnetic axis from R_{ax}=3.5 m, inward configuration, to 4.1 m, outward LHD configuration.

2.1 Broad pressure profile and field line in bad curvature region ($\theta_k = \alpha = 0$)

Constant growth rate lines γ normalized by τ_A, Alfven time, are shown in Fig. 1 versus β_0 and normalized radius ρ. Information of the most important rational surfaces and averaged magnetic well $d^2V/d\psi_N^2 = 0$ location is added in the plot. Mercier criterion stability lines are also plotted, like zero and positive (unstable) Mercier lines. Mercier criterion predicts instability for $R_{ax} \leq 3.7$ m, and stability for outward $R_{ax} > 3.7$ m configurations, it is said, interchange modes are unstable in inward configurations and stable in outward configurations. Ballooning growth rate study agrees with Mercier prediction in the inward configurations, but in outward configurations, near the plasma edge, MHD activity is reported. For $R_{ax} = 3.9$, the unstable region predicted by the Mercier criterion is narrow compared with the high n activity region. For $R_{ax} > 3.9$ m, all region is Mercier stable but the study of high n growth rate shows an important MHD activity. The position of low m/n rational surfaces is added to the plot. This allows us to follow the instability onset for each rational surface. For high beta, at the edge, the most unstable regions are related to $m/n = 2/3, 2/5$ and $1/2$ rational surfaces. For lower beta configurations and near the core, the $1/2$ rational surface dominates. This behaviour does not change for the rest of magnetic axis configurations except for $R_{ax} = 4.0$ m and 4.1 m, where the $1/2$ and $2/5$ rational surfaces will be related with the most unstable regions for high beta at the edge.

Average magnetic well null value location is also shown in Fig. 1. For inward configurations, $R_{ax} = 3.5$ m and 3.6 m configurations, $d^2V/d\psi_N^2 = 0$ line divides minor radius in two regions, the inner (outer) part where averaged magnetic well (hill) is located. This is because in averaged magnetic hill regions, averaged bad curvature, interchange modes are easily perturbed while in regions of magnetic

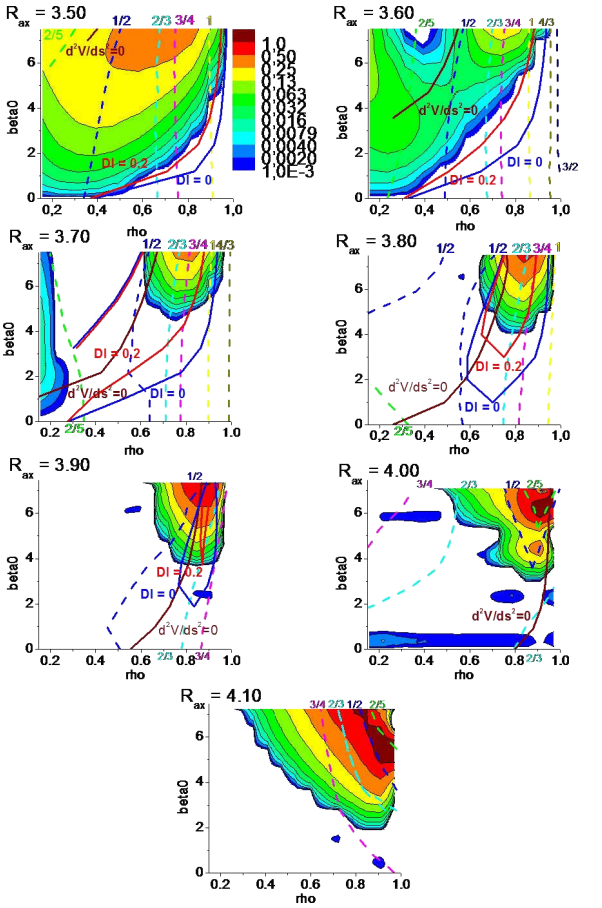

Fig. 1 Constant growth rates lines in a β_0 - ρ plane for different magnetic axis positions from $R_{ax} = 3.5$ to $R_{ax} = 4.1$ m. The pressure profile is broad and the field line is in bad magnetic curvature region.

well, averaged good curvature, interchange modes are stable. The $d^2V/d\psi_N^2 = 0$ line drifts to the edge as R_{ax} increases and magnetic well region reaches the periphery. For outward configurations there are large growth rates in the magnetic well region; only the local bad curvature and not the averaged bad curvature could be the driver of this instability, i.e., they are ballooning modes destabilized in local bad curvature regions near the plasma periphery.

In Fig. 2, the normalized radial position is fixed and constant Mercier criterion parameter lines and growth rate lines are shown for several magnetic axis configurations versus different beta values. Mercier criterion and growth rate study predicts interchange activity in the inner part of the torus, $\rho = 0.3$ and $\rho = 0.5$, but at the plasma edge in $\rho = 0.8$ for outer magnetic axis configurations for high beta, strong MHD activity is reported in a stable Mercier region.

2.2 Growth rate for field line in good magnetic curvature region ($\theta_k = 0$, $\alpha = \pi/M$)

We make again the study in good magnetic curvature region because, if the MHD activity is ballooning like,

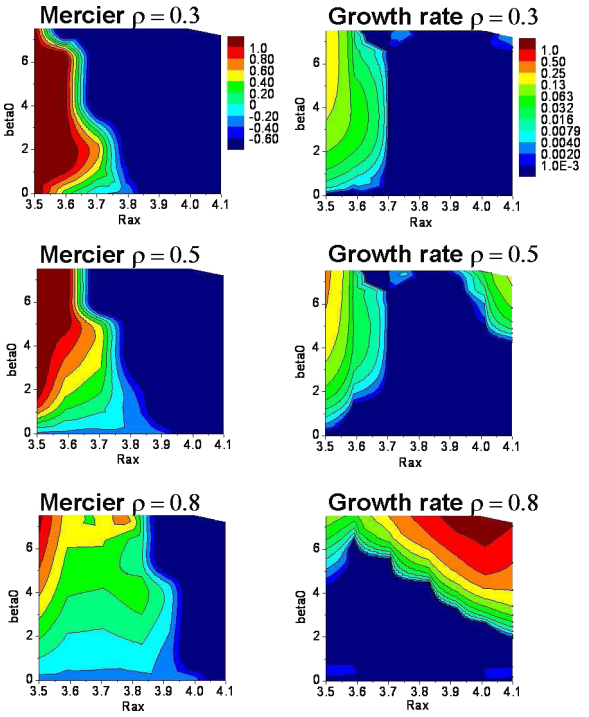

Fig. 2 Constant Mercier criterion lines (left) and constant high n mode growth rate lines (right) for broad pressure equilibrium. They are plotted in a β_0 - R_{ax} plane for three values of normalized radius.

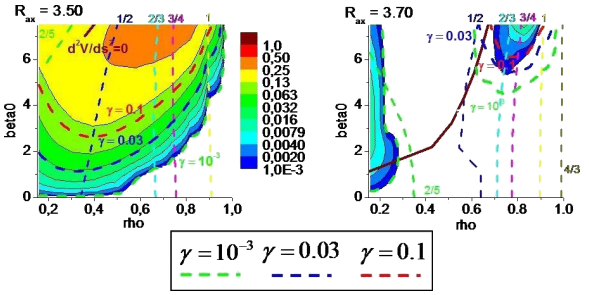

Fig. 3 Constant growth rates lines in a β_0 - ρ plane for field lines in good curvature regions. Constant growth rates lines for field lines with bad curvature are also represented by $\gamma = 10^{-3}$ line (marginal stability), $\gamma = 0.03$ (slightly unstable) and $\gamma = 0.1$ (unstable).

these modes are stabilized because their main driver, the curvature, is now favourable.

Figure 3 shows the high n ballooning behaviour for field lines in the good curvature region. For $R_{ax} = 3.5$ m, the behaviour is similar for good and bad curvature lines, i.e., this is an interchange mode. But for $R_{ax} > 3.5$ m the results begin to differ, as can be seen in $R_{ax} = 3.7$ m figure, where the growth rates for the good curvature field lines are lower than bad curvature ones, and for $R_{ax} > 3.7$ m high n balooning modes are stable. Other graphs with $R_{ax} > 3.7$ m are not shown because the growth rates for high n modes and Mercier criterion predict stability, even for outward

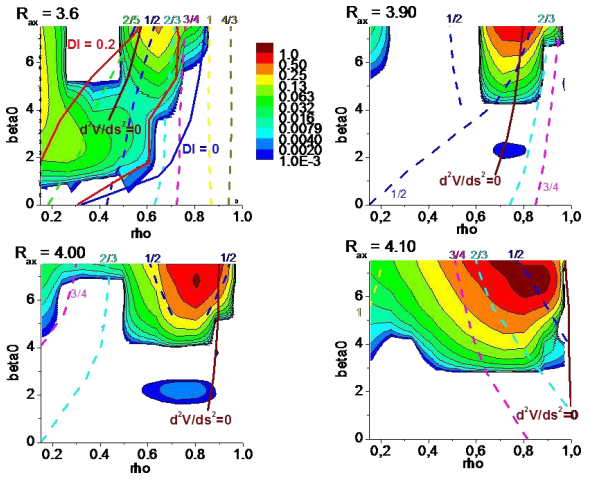

Fig. 4 Constant growth rates lines in a β_0 - ρ plane. They are plotted for four drifted magnetic axis positions. The pressure profile is peaked and the field line is in bad magnetic curvature region.

configurations with $R_{ax} = 4.1$ m. This result points out the instability is ballooning like.

2.3 Peaked pressure profile and field line in bad curvature region ($\theta_k = \alpha = 0$)

Similar analysis of Sec. 2.1 has been done for equilibria with peaked pressure profile. The results are similar to broad pressure equilibriums, and conclusions are the same (Fig. 4). Broad pressure equilibriums are more unstable under ballooning activity, and its strongest activity is reached for $\beta_0 = 5\%$ while peaked one at $\beta_0 = 6\%$. Another conclusion is that, for broad equilibriums, the ballooning activity is strongly located in the edge but the peaked ones are spread more widely along minor radius.

With respect to the behaviour at regions close to the rational surfaces, 2/3 and 1/2 are the most unstable rational surfaces for high beta at the edge for inward magnetic axis configurations. The growth rates at the rational surfaces 3/4 and 2/5 are smaller. The highest high n modes activity in outward magnetic axis configuration is related to rational surface 1/2. The behaviour of the $d^2V/d\psi_N^2 = 0$ line is similar to the broad cases; for inward configurations there is stability in the inner part of the minor radius and instability in the outer part for inward magnetic axis configurations, interchange modes are unstable in regions with averaged bad magnetic curvature, but in outward configurations the $d^2V/d\psi_N^2 = 0$ line is drifted to the edge and good averaged curvature region reaches the plasma periphery where the high n ballooning modes are unstable.

Figure 5 shows the same study at fixed radial position. Inward and outward configuration have similar high n ballooning activity for $\rho = 0.3$ and $\rho = 0.5$, but near the edge at $\rho = 0.8$, peaked pressure equilibriums have its maximum ballooning activity for configurations with the magnetic axis located between $R_{ax} = 4.0$ and $R_{ax} = 4.1$ but

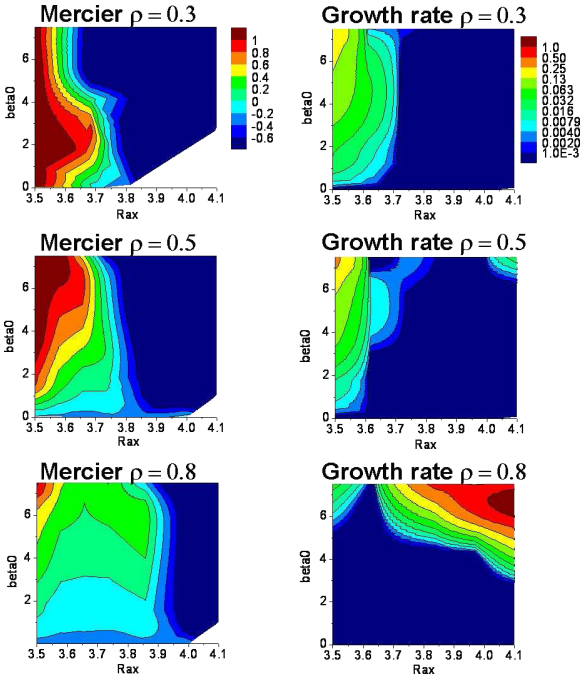

Fig. 5 Constant Mercier criterion lines (left) and constant high n mode growth rate lines (right) for peaked pressure equilibrium. They are plotted in a β_0 - R_{ax} plane for three values of normalized radius.

the broad ones between $R_{ax} = 3.9$ and $R_{ax} = 4.1$

3. Conclusions and Discussion

High n mode stability properties have been studied for several beta and magnetic axis configurations. By analyzing the growth rates of high n modes for outward configurations, in regions with bad magnetic curvature, we have seen that instabilities are triggered in Mercier stable regions and show dependence versus curvature, a characteristic behaviour of ballooning modes. For inward configurations, modes are not destabilized by local bad magnetic curvature and high n modes activity is located in Mercier unstable regions, properties of interchange instabilities.

This study was made for broad and peaked pressure profiles, and the results show for the growth rate at $R_{ax} = 4.1$ m, Figs. 1 and 4, that in broad pressure profile the most unstable region is more narrow, located in the edge of plasma ($\rho = 0.9$-1.0) and the beta value where growth rate reachs its maximum is around $\beta_0 > 5\%$, compared with peaked pressure profile, where the most unstable region is located between $\rho = 0.7$-0.9 and for $\beta_0 > 6\%$. Studying Figs. 2 and 5, for broad profiles the strongest unstable region is more concentrated in the peripheral region and is triggered from $R_{ax} = 3.9$ m magnetic axis configurations while peaked ones are spread more widely along minor radius and triggered from $R_{ax} = 4.0$ m.

The aim of the study was to reveal the properties of MHD activity found in LHD operation for outward configurations. Reference [7] shows that peaked pressure equilibria results point out that 3D ballooning modes strongest growth rate is related with the operation region where density collapse events are driven, so present simulation has a direct relation with LHD experimental data.

Appendix

The ballooning equation solved in the code is [2]:

$$\frac{2}{B_0}\left(\frac{J}{\iota B}\right)^2 \frac{\mathrm{d}p}{\mathrm{d}\psi}\left[\kappa^n - \kappa_g \int^{\eta} \hat{s}\,\mathrm{d}\eta\right]\Phi + \frac{\partial}{\partial\eta}\left[|k_\perp|^2 \frac{\partial}{\partial\eta}\Phi\right] + \Omega^2\left(\frac{\langle B\rangle^2}{B^2}\right)|k_\perp|^2\Phi = 0 \quad (1)$$

where $\Omega = \omega\tau_A$ are the eigenfrequency normalized by the Alfven time τ_A, given by $\tau_A^2 = \rho_m/[2\pi\iota(\mathrm{d}\Phi_n/\mathrm{d}V)]^2$. p is the pressure, V the volume, $k_\perp$ the perpendicular wave number, Φ_N the normalized toroidal flux inside the flux surface ψ with $\Phi_N = 2\pi\psi_N$ with $\rho = \sqrt{\psi_N}$, ι the global rotational transform and $\hat{s}$ the local magnetic shear. κ^n is the contravariant form of the normal magnetic curvature, and is expressed like [2]:

$$\kappa^n = \frac{2\psi\vec{\kappa}\cdot\vec{\nabla\psi}}{|\nabla\psi|^2} \quad (2)$$

and κ_g the geodesic magnetic curvature as:

$$\kappa_g = \frac{B^2}{2}\frac{\partial}{\partial\theta}\left(\frac{1}{B^2}\right). \quad (3)$$

This problem has been solved by other authors in different devices [11–13], but this code was selected to be an optimized common tool used in the LHD ballooning modes research.

The Mercier criterion parameter (DI) expresion is [2]:

$$DI = \frac{\iota'^2}{4} - \frac{p'V'}{(2\pi)^2}\left[-\left\langle\frac{B^2}{|\nabla\psi|^2}\right\rangle V'' + \left\langle\frac{(\boldsymbol{j}\cdot\boldsymbol{B})_{PSN}}{|\nabla\psi|^2}\right\rangle\iota'\right] + \left(\frac{p'V'}{2\pi}\right)^2\left[\frac{1}{(2\pi)^2}\left\langle\frac{(\boldsymbol{j}\cdot\boldsymbol{B})^2_{PSN}}{|\nabla\psi|^2B^2}\right\rangle\left\langle\frac{B^2}{|\nabla\psi|^2}\right\rangle\right] + \left(\frac{p'V'}{2\pi}\right)^2\left[\left\langle\frac{(\boldsymbol{j}\cdot\boldsymbol{B})_{PSN}}{|\nabla\psi|^2}\right\rangle - \left\langle\frac{B^2}{|\nabla\psi|^2}\right\rangle\left\langle\frac{1}{B^2}\right\rangle\right] \quad (4)$$

where $(\boldsymbol{j}\cdot\boldsymbol{B})_{PSN} = -2\pi\boldsymbol{B}\wedge\nabla\psi\cdot\nabla\tilde{\beta}_N \equiv$ Pfirsch-Schlüter current divided by p', $\boldsymbol{B}\cdot\nabla\tilde{\beta}_N = 1 - B^2/\langle B^2\rangle$, $\langle f\rangle = (\mathrm{d}/\mathrm{d}V)\int f\mathrm{d}\tau \equiv$ average over flux surface and $A' = [(1/2\pi)(\mathrm{d}/\mathrm{d}\psi)]A$. The first equation element is a stabilizing term by the magnetic shear effect, the second term can be stabilizing or destabilizing depending on the magnetic shear and the averaged magnetic hill sign, and the last one is destabilizing and includes Pfirsch- Schlüter current, geodesic curvature and diamagnetic current effects.

[1] H. Yamada *et al.*, Plasma Phys. Control. **43**, A53 (2001).
[2] N. Nakajima, Phys. Plasmas **3**, 4556 (1996).
[3] N. Nakajima, S.R. Hudson and C.C. Hegna, Fusion Sci. Technol. **51**, 79 (2007).

[4] J. Chen, N. Nakajima and M. Okamoto, Phys. Plasmas **6**, 5 (1999).
[5] C. Schwab, Phys. Fluids B **5**, 3195 (1993).
[6] C. Nührenberg, Phys. Plasmas **6**, 137 (1999).
[7] S. Ohdachi *et al.*, Contrib. Plasma Phys. **50**, 552 (2010).
[8] S.P. Hirshman and J.C. Whitson, Phys. Fluids **26**, 3553 (1983).
[9] C. Mercier, *Commission of the European Communities* (1974).
[10] N. Nakajima, Phys. Plasmas **3**, 4545 (1996).
[11] R. Sanchez *et al.*, Nucl. Fusion **37**, 3557 (1997).
[12] R. Sanchez *et al.*, J. Comput. Phys. **161**, 567 (2000).
[13] W.A. Cooper *et al.*, Nucl. Fusion **29**, 617 (1989).
[14] O. Motojima *et al.*, Nucl. Fusion **45**, S255 (2005).
[15] K.Y. Watanabe *et al.*, Nucl. Fusion **45**, 1247 (2005).
[16] M. Yu Isaev, K.Y. Watanabe *et al.*, Nucl. Fusion **49**, 075013 (2009).
[17] L. Brocher *et al.*, Nucl. Fusion **50**, 025009 (2010).
[18] E.A. Veshchev *et al.*, J. Plasma Fusion Res. **5**, S1024 (2010).
[19] V.D. Shafranov, Rev. Plasma Phys. **2**, 103 (1966).
[20] V.D. Shafranov, Sov. Phys. J.E.T.P **6**, 54 (1957).
[21] N. Nakajima, Nucl. Fusion **46**, 177 (2006).